INTRODUCTION

Air cooling is still the most attractive method for computer systems and other electronic equipment. due to its simplicity and low cost. Thermal engineers in the electronics industry are always trying to achieve the best possible performance out of air cooling. In this effort, the need for understanding the variety of flow phenomena and convective heat transfer mechanisms that are present in air-cooled electronic systems is obvious.

Extensive surveys of the various modes of convective heat transfer and relevant configurations along with the associated heat transfer correlations have been presented by Jaluria [1], Papanicolaou and Jaluria [2], and El Kady [3]. Large number of practical situations involve mixed convective heat transfer in which both modes of forced and natural convection effects are dominant and both modes are significant. Such circumstances arise when a fluid flows over a heated surface with relatively low velocity. The effect of the incorporation of both transport mechanisms on the heat transfer rate is particularly important in the design of thermal systems, such as electronic circuitry and furnaces. In the work of Habchi and Archarya [4] a numerical study was done for mixed convection of air in a vertical channel containing partial rectangular blockage on one channel wall. The wall containing the blockage was assumed to be heated while the other wall was assumed to be adiabatic or heated. Maughan and Incropera [5] made experimental measurements in the thermal entry for various channel inclinations. Kang et. al. [6] obtained experimental results for the cooling of a protruding heat generating module on a horizontal plate in an externally induced forced flow. Mahaney et al. [7] studied the mixed convective heat transfer from an array of discrete heat sources in a horizontal rectangular channel. An analysis is made by Kim et. al. [8] of the flow and heat transfer characteristics of a mixed convection from multiple-layered boards with cross-streamwise periodic boundary conditions. Papanicolaou and Jaluria [2] studied numerically the combined forced and natural convective cooling of heat dissipating surface electronic components. located in the walls of a rectangular cavity, and cooled by an upper external through flow of air.

These studies illustrated the lack of knowledge in mixed convection from protruding heat sources. The present study is directed to develop numerical model to investigate the fluid flow and heat transfer characteristics due to the mixed convection from protruding heat source in rectangular channels. The dependence of the heat flow characteristics on the distance of the heater from the inlet section of the air flow is investigated. The ranges of the natural convective dominated flow, transient and forced convection dominated flow are determined as a function of the strength of the mixed convection Richardson number Gr/Re^2. Correlations for the average Nusselt number and maximum heater surface temperature are developed as a function of Gr/Re^2. Experimental test was done and the results were used to validate the numerical model.

MATHEMATICAL FORMULATION AND METHOD OF SOLUTION

A laminar mixed convection air flow is considered in a horizontal channel of height H. The channel contains a protruding heat source of length L and height b with output uniform heat flux q, placed on the lower horizontal channel wall, as illustrated in

Fig. 1. External air enters the channel with uniform velocity u_o and constant ambient temperature T_o. The horizontal surface carrying the heat source is maintained adiabatic, while the top channel surface is maintained at the ambient air temperature T_o. Assuming that the fluid properties are constant except for density, the governing equations for mass, momentum with the Bousinesq approximation and energy in the channel are:

$$\partial u/\partial x + \partial w/\partial y = 0 \quad (1)$$

$$u\,\partial u/\partial x + v\,\partial u/\partial y = -\,1/\rho.[\partial P/\partial x] + \upsilon.[\partial^2 u/\partial x^2 + \partial^2 u/\partial y^2] \quad (2)$$

$$u\,\partial v/\partial x + v\,\partial v/\partial y = -\,1/\rho.[\partial P/\partial y] + \upsilon.[\partial^2 v/\partial x^2 + \partial^2 v/\partial y^2] + g\beta(T - T_o) \quad (3)$$

$$u\,\partial T/\partial x + v\,\partial T/\partial y = \alpha.[\partial^2 T/\partial x^2 + \partial^2 T/\partial y^2] \quad (4)$$

where u, v, P, T, ρ, υ, β, and α are the velocity in the horizontal and vertical directions x and y, pressure, fluid temperature, the fluid density, the fluid kinematic viscosity, fluid coefficient of thermal expansion and the thermal diffusivity respectively.

Eliminating the pressure P between equations (1) and (2), from definitions $\zeta=\partial v/\partial x-\partial u/\partial y$, $u=\partial\psi/\partial y$ and $v=-\partial\psi/\partial x$ and using the nondimensional variables: $X=x/L$, $Y=y/L$, $U=u/u_o$, $V=v/u_o$, $\omega=\zeta.L^2/\upsilon$, $\Psi=\psi/\upsilon$ and $\theta=(T-T_o)/(q.L/k)$ the dimensionless form for the governing equations (1-4) can be written in terms of nondimensional stream function, vorticity, horizontal and vertical velocities, and temperature as follows:

$$U.\partial\omega/\partial X + V.\partial\omega/\partial Y = 1/Re.\,[\partial^2\omega/\partial X^2 + \partial^2\omega/\partial Y^2] + Gr/Re^2\,.\,[\partial\theta/\partial X] \quad (5)$$

$$-\omega = \partial^2\Psi/\partial X^2 + \partial^2\Psi/\partial Y^2 \quad (6)$$

$$U.\partial\theta/\partial X + V.\partial\theta/\partial Y = 1/(Pr.Re)\,.\,[\partial^2\theta/\partial X^2 + \partial^2\theta/\partial Y^2] \quad (7)$$

$$U=\partial\Psi/\partial Y \text{ and } V=-\,\partial\Psi/\partial X \quad (8)$$

where Grashof number $Gr = g\beta\,L^4\,q\,/k\upsilon^2$, Reynolds number $Re = u_o L/\upsilon$, Prandtl number $Pr = \upsilon/\alpha$ and k is the fluid thermal conductivity.

The dimensionless boundary conditions can be expressed as:

$$\text{at } X = 0:\ U = 1,\ V = 0,\ \theta = 0 \quad (9a)$$

$$\text{at } Y=0,\ 0<X\le L_1/L,\ 1+L_1/L\le X\le 1+(L_1+L_2)/L:\ U = V = 0\ ,\ \partial\theta/\partial Y = 0 \quad (9b)$$

$$\text{at } Y=H/L,\ 0\le X\le 1+(L_1+L_2)/L:\ U = V = \theta = 0, \quad (9c)$$

$$\text{at } X=1+(L_1+L_2)/L,\ 0\le Y\le H/L:\ \partial U/\partial X = \partial V/\partial X = \partial\theta/\partial X = 0 \quad (9d)$$

$$\text{at heater surface, } Y= b/L,\ L_1/L\le X\le 1+(L_1/L):\ U = V = 0,\ \partial\theta/\partial Y = -1 \quad (9e)$$

$$\text{at } X= L_1/L,\ 0\le Y\le b/L:\ U = V = 0,\ \partial\theta/\partial X = 1 \quad (9f)$$

$$\text{at } X= 1+L_1/L,\ 0\le Y\le b/L:\ U = V = 0,\ \partial\theta/\partial X = -1 \quad (9g)$$

The local and average heat transfer coefficients along the surface of the heater are presented by means of the Nusselt number and may be expressed in terms of the measured flux and temperatures according to the definition used in [4] and [6] as:

$$Nu = h.L/k = (q.L/k)/(T - T_o) \quad (10)$$

$$\bar{N}u = (q\,L/k)/(\bar{T} - T_o)] \quad (11)$$

where $\bar{T}$ is the average heater surfaee temperature.

The dimensionless governing equations (5)-(8) and the associated boundary conditions given by equation (9) were solved by a finite difference procedure discussed by Patanker [9]. The domain is subdivided into a number of control volumes, each associated with a grid point, and the governing equation is integrated over each control

volume resulting in a system of algebraic equations which are solved using the Gauss-Seidel elimination method. An iterative solution procedure was employed here to obtain the steady state solution of the problem considered. The calculations were done on finer grid size distributions. A 31x121 uniform grid was considered to give grid independent results. The convergence criteria used for all field variables $\xi(=\omega, \Psi, \theta)$ for every point is $\left|(\xi^{n+1}-\xi^{n})/\xi^{n}\right|_{max} \leq 10^{-5}$ where n is the index representing the iteration number.

EXPERIMENTAL WORK

A low speed wind tunnel, with 12x12cm square cross section of wood and 60 cm long is used. The air enters the test section (1) shown in Fig. 2 through a bell mouth (2) and a fine mesh screen (3) to ensure a fairly uniform flow with a negligible turbulence in the test section. The local flow velocity is measured by means of a hot wire anemometer (4) at different locations in both the Y and Z directions at a section free of the block heater and is integrated to get the average air velocity. A nickel-chromium heater wire (5) is wrapped at equal pitches over a three sides of backalite core of 2.2 cm wide, 1.4 cm beight and 12 cm long (6). This core is surrounded by mica sheets of 0.5 mm thickness (7) and is inserted inside a highly polished aluminum channel of 2.7 cm wide, 1.6 cm height and 12 cm long (8) to form the heat source module (9). The heat source module is fixed on the floor of the channel which is made of 5 cm thickness wood. The heat input to the heater is controlled by using an auto-transformer (10) as well as an ammeter (11) and voltmeter (12). The heater surface temperature is measured by nine copper-constantan thermocouples (13), while the temperature distribution along the floor is measured hy 15 thermocouples. The thermocouples are connected to a Yokogawa digital temperature recorder with a sensitivity of 0.1°C. Nearly one hour was needed to reach the steady state condition.

To validate the numerical calculated results, experimental tests were done for geometrical dimensions of $L_1/L=11$, $L_2/L=10$, $b/L=0.6$ and $H/L=7.3$ and operating parameters of $Pr=0.7$, $Gr=5.5\times10^6$ and $Re= 374, 816, 1200$ and 1500. Comparisons are shown in Figs. 3 and 4 between the calculated local surface temperature and heater local Nusselt number with the experimental results. Fair agreement exists with average and maximum differences of 6 and nearly 9 percent, respectively.

RESULTS AND DISCUSSION

The dependence of the beat flow characteristics on tbe distance of the protruding heater from the inlet section of the channel is studied. Also tbe regions of the natural convective dominated flow, transient flow and forced convection dominated flow are determined in terms of the Reynolds number and the mixed convection Richardson number Gr/Re^2. The geometrical particulars were set forth: $L=1$, $b/L=0.5$, $0.5\leq L_1/L\leq 6$, $1\leq L_2/L\leq 6.5$, and $H/L=2$. The operating parameters are $Pr = 0.7$, $Re\leq 10^3$, and Gr/Re^2 up to 10^4. The results are presented in the form of streamline and isotherm contours, temperature profiles at the heater surfaces. Heat transfer results are presented as the local and average Nusselt number at the heater surfaces.

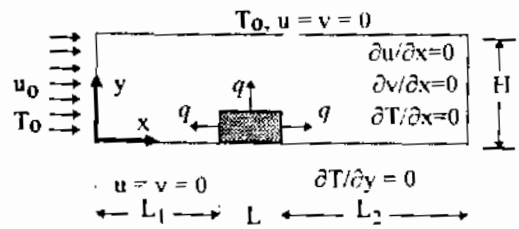

Fig. 1 Physical model, coordinate system and boundaries

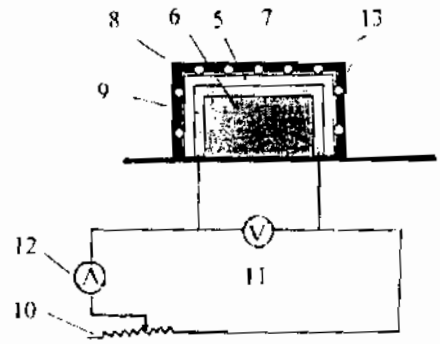

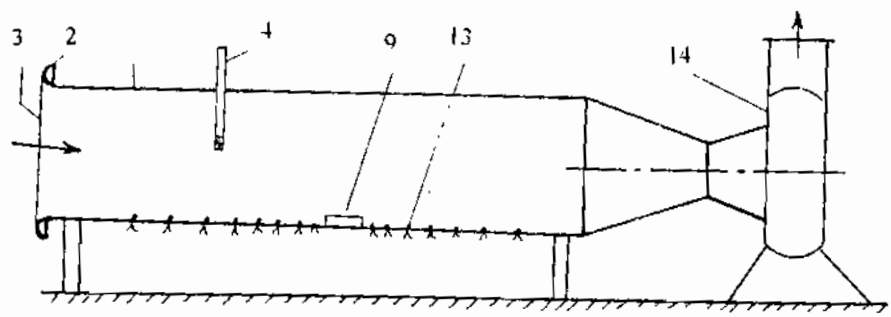

Fig. 2 Schematic diagram of the experimental apparatus

(1) Test section, (2) bell mouth, (3) fine mesh screen, (4) hot wire anemometer, (5) nickel-chromium electric heater, (6) backalite core , (7) sheet of mica, (8)Aluminuim channel, (9) heat source module, (10) auto transformer, (11) voltmeter, (12) ammeter, (13) copper-constantan thermocouple, and (14) blower

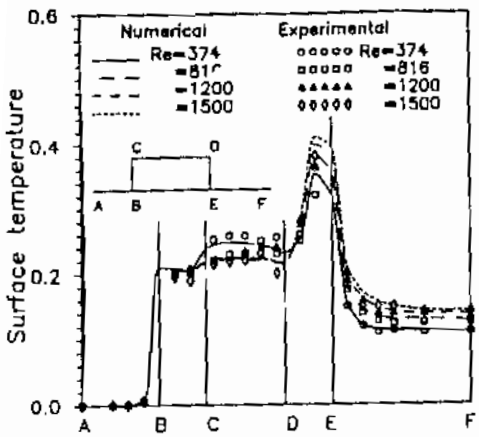

Fig. 3 Comparison between the numerical and experimental heater surface temperature for L_1/L=11, L_2/L= 10, b/L=0.6, H/L=7.3 and Gr = $5.5x10^6$

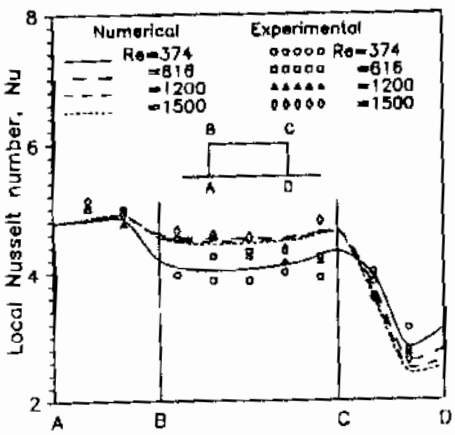

Fig. 4 Comparison between the numerical and experimental heater surface local Nusselt number for L_1/L=11, L_2/L= 10, b/L=0.6, H/L=7.3 and Gr = $5.5x10^6$

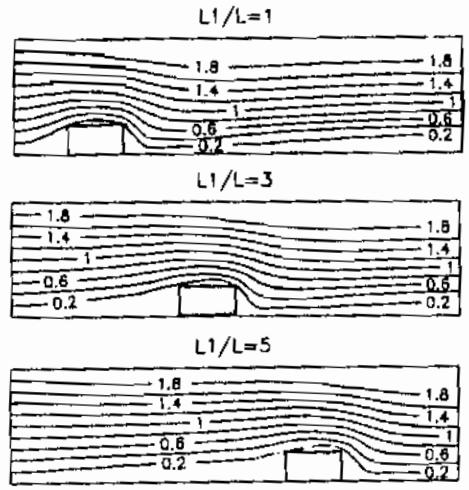

Fig. 5 Influence of heater location on the streamlines for b/L=0.5, H/L=2, Pr =0.7, Re=250, Gr=10^6 and Gr/Re^2=16

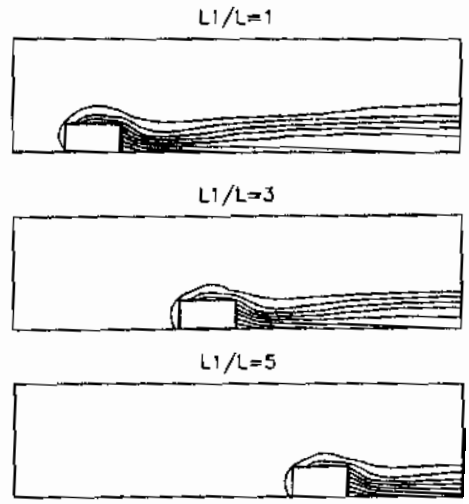

Fig. 6 Influence of heater location on the temperature contours for b/L=0.5, H/L=2, Pr =0.7, Re=250, Gr=10^6 and Gr/Re^2=16

Fluid flow Structure and Isotherms

The streamline and isotherm contours are presented in Figs. 5 and 6 for Re=250 and $Gr=10^6$. The fluid acts according to two forces, the external forced air flow velocity and the buoyancy due to the heat dissipation from the heater. As the flow approaches the heater, the streamlines are deflected towards the upper horizontal channel surface. Therefore, the streamlines above heater are more densely packed. Downstream the heater, the flow separates and reattaches further on the floor surface making denser flow region near the channel floor surface and lower density flow near the channel upper surface. In Fig. 6, the boundary layer thickness changes rapidly near the heater because of the influence of the heater blockage on the distortion of the external flow and on the resulting temperature distribution in the flow over the heater. Fig. 6 shows the upstream penetration and the downstream spread and decay of thermal effects. Downstream of the heater, the boundary layer thickness keeps on increasing gradually, because of the wake effect in the flow and owing to the fact that the thermal buoyancy force is normal to the external flow direction.

Heater Surface Temperature

The reliability and operation of electronic components depends on the maximum temperature attained by the component. Figure 7 displays the local temperature θ distribution along the heater surfaces A-B, B-C, and C-D for Re=250 and $Gr=10^6$. θ is minimum at a point nearer to point B. It increases gradually towards the bottom corner at point A which has the maximum temperature of the left face A-B. For the purely natural convection case, the location of θ_{max} at the top heater surface (B-C), is at the center point. In the studied mixed convection case, Fig. 7 shows a deviation of θ_{max} location from the heater center, owing to the existence of the external forced air flow. At the right face θ increases in the direction towards the bottom corner due to the flow separation and wake effects making θ_{max} at point D.

The variation of θ_{max} with the L_l/L ratio is shown in Fig. 8. It is shown that θ_{max} of the right face (surface C-D) is found to be the largest due to the separation of the flow and wake region effects near it. While θ_{max} at the left face (surface A-B) is always found to be the lowest this surface is facing to the external colder flow.

Heat Transfer

The distribution of the local Nusselt number Nu along the heater surfaces is shown in Fig. 9 for Re=250 and $Gr=10^6$. Nu is seen to increase up to the top corner of the left face (A-B). A maximum of Nu is observed near this corner, followed by a gradual decay at the top face (B-C) until the point of maximum temperature, then followed by another gradual increase until the trailing edge of the top surface. At the right face C-D, a gradual decrease is observed from the top corner point to the bottom corner point, making point D to have the minimum rate of heat transfer.

$\bar{Nu}$ is shown versus L_l/L in Fig. 10. $\bar{Nu}$ at the left face (surface A-B) is found to be the largest among the three faces since this surface is facing the external air flow. While $\bar{Nu}$ at the right face (surface C-D) is the lowest among the three faces due to the separation of the flow and wake region effects.

Effect of heater Location

The influence of the heater module location in the channel (the distance between the heater and the entrance section of the channel L_1/L) on the flow and heat transfer characteristics is shown in Figs 5-10 for Re =250, Gr=10^6, b/L=0.5, and $0.5 \leq L_1/L \leq 6$. Figures 5 and 6 show no clearly influence of the position of the heater module L_1/L on the streamline or isotherm contours before, over or after the heater module. With the increase of L_1/L ratio, an increase of the surface temperature of the left surface A-B which is shown in Fig. 7 and a decrease of the local Nu which is shown in Fig. 9 for L_1/L =1 and 2. For $L_1/L>2$, no change in both θ and Nu exists. With the increase of L_1/L, small decrease exists in θ and increase of the Nu at the top heater surface (B-C). For the right heater surface (C-D), both θ and Nu are insensitive for the change of the L_1/L ratio. The ratio $L_1/L \leq 2$ is the best region for the location of the heater module because of the relatively higher values of the average Nusselt number for the three heater surfaces expressed by (A-B-C-D), as shown in Fig. 10. For $L_1/L>2$, θ_{max} as well as $\bar{Nu}$ for the right, top and left heater surfaces are nearly constant.

Effect of operating parameters

Figures 11 and 12 present the variation of θ_{max} and $\bar{Nu}$ with Rc for the three heater faces for L_1/L=2, b/L=0.5, H/L=2, Gr= 10^6 and $10 \leq Re \leq 10^3$. θ_{max} at the right, top, and left surfaces of the heater decrease as shown in Fig. 12 with the increase of Reynolds number up to Re=70. For $70 \leq Re \leq 140$ the changes of θ_{max} occur with smaller rates. This is the transition region from a natural convection dominated flow to a forced convection dominated one. The above transition in the flow has a big influence on θ_{max}. For Re>140, θ_{max} at the right face (A-B) and left face (C-D) of the heater, increases with smaller rates which makes the values of θ_{max} at Re=10^3 still less than its smallest values at the end of the natural convection dominated flow region. For the top surface (B-C), θ_{max} decreases with the increase of Reynolds number. Figure 12 shows the behavior of $\bar{Nu}$ for the three faces of the heater module with the increase of Reynolds number. In the natural convection dominated flow, $\bar{Nu}$ for the three heater faces increases with increasing of Re. A slower increase in $\bar{Nu}$ is observed during the transition, followed by gradual increase in the forced convection dominated region for both the left and the top faces and nearly no change in $\bar{Nu}$ at the right face. These results indicate that flow velocity that puts the flow in the forced convection dominated region, just outside the transition region, is recommended.

The variation of θ_{max} and $\bar{Nu}$ with Gr/Re^2 are shown in Figs. 13 and 14. The results indicate that the flow is a forced convection dominated flow when $Gr/Re^2 \leq 51$, transient by $51 \leq Gr/Re^2 \leq 204$ and a natural convection dominated one when $Gr/Re^2 \geq 204$. To obtain the dependence of both θ_{max} and $\bar{Nu}$ on Gr/Re^2, correlations were expressed for the three heater surfaces as follows:

$$\theta_{max} = a\,(Gr/Re^2)^b \quad \text{and} \quad \bar{Nu} = c\,(Gr/Re^2)^d \qquad (12)$$

where a, b, c, and d are constants shown in the following table.

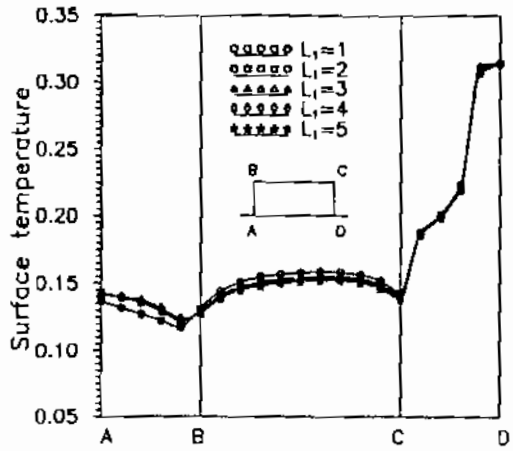

Fig. 7 Influence of heater location on the local temperature for b/L=0.5, H/L=2, Pr = 0.7, Re=250, Gr=10^6 and Gr/Re^2=16

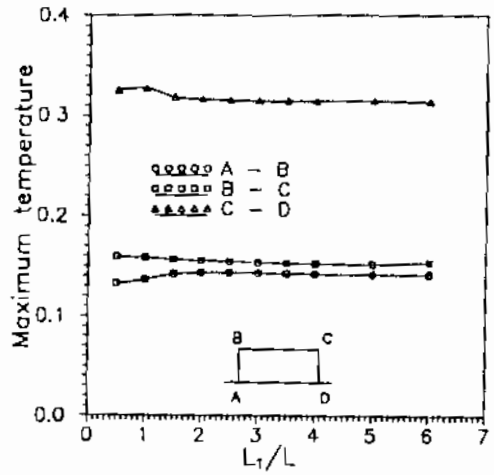

Fig. 8 Influence of heater location on the maximum temperatures for b/L=0.5, H/L=2, Pr=.7, Re=250, Gr=10^6 and Gr/Re^2 =16

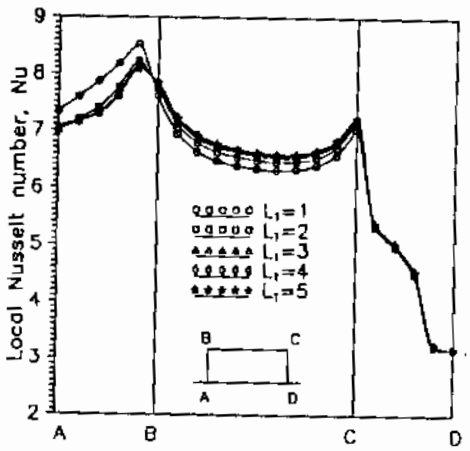

Fig. 9 Influence of heater location on the local Nusselt number for b/L=0.5, H/L=2, Pr= 0.7, Re=250, Gr=10^6 and Gr/Re^2=16

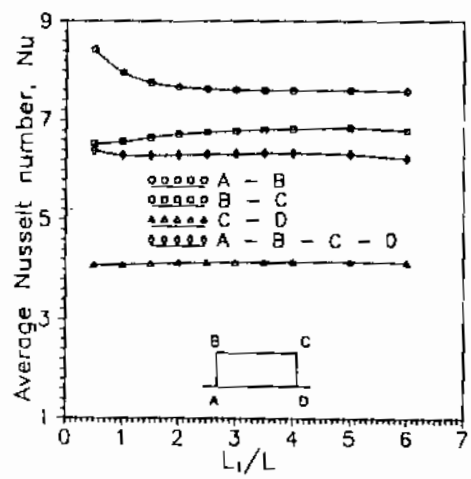

Fig. 10 Influence of heater location on the average Nusselt number for b/L=0.5, H/L=2, Pr =0.7, Re=250, Gr=10^6 and Gr/Re^2 =16

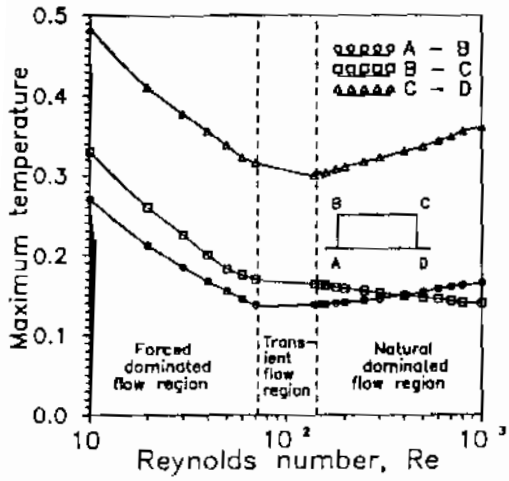

Fig. 11 Variation of maximum heater surfaces temperature with Reynolds number for b/L=0.5, H/L=2, Pr= 0.7, and Gr=10^6

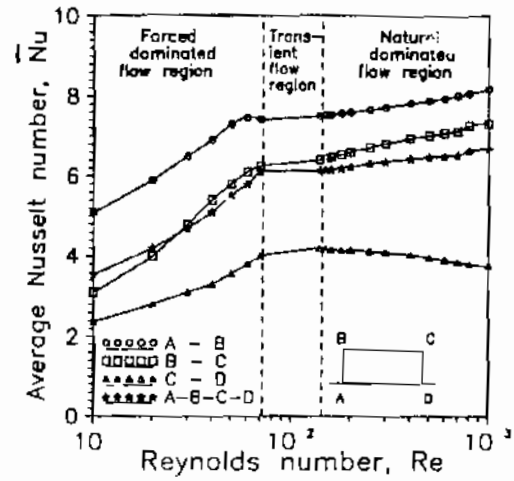

Fig. 12 The variation of the average Nusselt number with Reynolds number for b/L=0.5, H/L=2, Pr= 0.7, and Gr=10^6

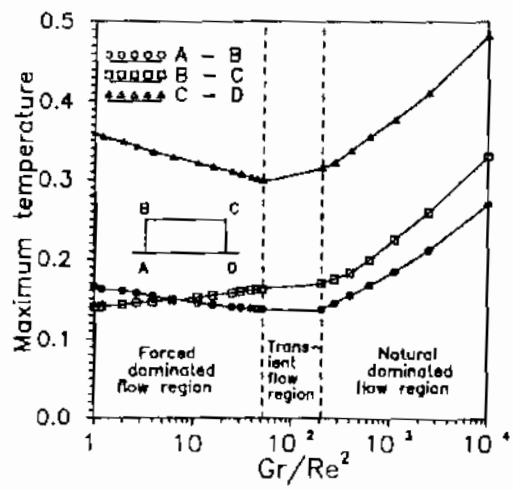

Fig. 13 The variation of maximum heater surfaces temperature with strength of mixed convection for b/L=.5, H/L=2 and Pr= 0.7

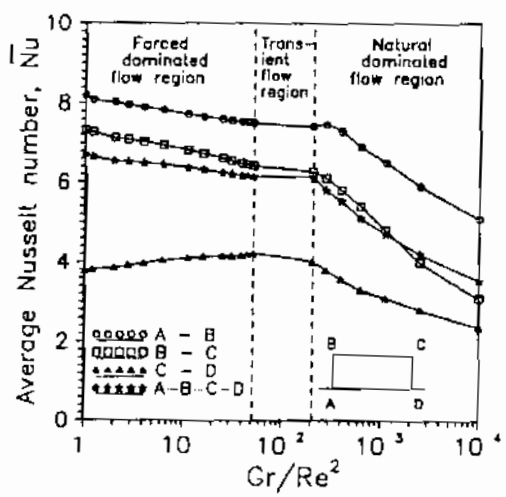

Fig. 14 The variation of the average Nusselt number with the strength of mixed convection for b/L=.5, H/L=2 and Pr= 0.7

heater surface	Forced convection dominated flow $Gr/Re^2 \leq 51$		Transient flow $51 \leq Gr/Re^2 \leq 204$		Natural convection dominated flow, $Gr/Re^2 \geq 204$	
	a	b	a	b	a	b
A-B	0.165	-0.048	0.139	-0.0021	0.0547	0.173
B-C	0.14	0.039	0.1621	-0.0022	0.0628	0.171
C-D	0.359	-0.045	0.3356	-0.03156	0.174	0.111
	c	d	c	d	c	d
A-B	8.143	-0.021	7.769	-0.0085	13.95	-0.109
B-C	7.34	-0.034	6.886	-0.018	18.04	-0.1913
C-D	3.814	0.0256	4.823	-0.0352	8.00	-0.133
A-B-C-D	6.676	-0.0213	6.255	-0.0047	12.71	-0.1396

CONCLUSIONS

A numerical procedure was developed to simulate the mixed convection from a heat source protruding from the floor of a horizontal channel. The results show the following:

The thermal boundary layer thickness increases rapidly before, over, and downstream of the heater with an upstream penetration and a downstream spread and decay of thermal effects.

θ_{max} at the left and right heater faces occur at the bottom corner points, while, its location at the top surface depends on Gr/Re^2. θ_{max} of the right face of the heater is the largest temperature, while θ_{max} at the left face is the lowest one. $\bar{Nu}$ at the left face of the heater is the largest while, $\bar{Nu}$ at the right face is the lowest.

The ratio $L_1/L \leq 2$ is the best region for the location of the heater module because of the relatively higher values of the total average $\bar{Nu}$ for the three heater surfaces.

The forced convection dominated flow region is determined hy $Gr/Re^2 \leq 51$, the transient regionis determined hy the $51 \leq Gr/Re^2 \leq 204$, while, the natural convection dominated one is determined by $Gr/Re^2 \geq 204$. For the three regions θ_{max} and $\bar{Nu}$ for the three heater surfaces are correlated with Gr/Re^2 as:

$$\theta_{max} = a\,(Gr/Re^2)^b \quad \text{and} \quad \bar{Nu} = c\,(Gr/Re^2)^d$$

where a, b, c, and d are constants.

NOMENCLATURE

a,b,c,d	constants of Eq. (12)	u	air velocity in the x direction, m/s
b	heater height, m	v	air velocity in the y direction, m/s
Gr	Grashof number, $Gr = g\beta L^4 q / k\upsilon^2$	u_o	air temperature at entrance, m/s
h	convective heat transfer coefficient $W/m^2.K$	U,V	non-dimensional air velocity in th X and Y directions, u/u_o and v/u_o
H	channel height, m	x	distance in horizontal direction, m
k	fluid thermal conductivity, W/mK	y	distance in vertical direction, m

L	heater width, m	X,Y	dimensionless distance in x and directions, x/L and y/L
L_1	distance from the channel inlet, m	α	fluid thermal diffusivity, m^2/s
L_2	distance from the channel exit, m	β	fluid volumetric coefficient of thermal expansion, 1/K
Nu	local Nusselt number, Eqs.(10)	θ	dimensionless temperature
Nu	average Nusselt number, Eqs.(11)	ψ	stream function, m^2/s
P	pressure, Pa	Ψ	dimensionless stream function, ψ/υ
Pr	fluid Prandtl number, υ/α	ζ	vorticity, 1/s
q	heat flux on the heater surface, W/m^2	ω	nondimensional vorticity, $\omega=\zeta L^2/\upsilon$
Re	fluid Reynolds number, $Re = u_o L/\upsilon$	υ	fluid kinematic viscosity, m^2/s
T	fluid temperature, K	ρ	fluid density, kg/m^3
T_o	air temperature at channel entrance, K		

REFERENCES

1. Jaluria, Y., "Natural Convective Cooling of Electronic Equipment," in "Natural convection, Fundamentals & Applications" Kakac, S., Aung, V., and Viskanta, R., Hemisphere Publishing corporation, pp. 961-986, 1985.
2. Papanicolaou, E., and Jaluria, Y., "Mixed Convection From Simulated Electronic Components at Varying Relative Positions in a Cavity," ASME J. of Heat Transfer, Vol. 116, pp. 960-970, 1994.
3. El Kady, M. S., " Natural Convection From Dual Surface Heat Sources in a Vertical Rectangular Enclosure," Mansoura Engineering Journal (MEJ), Vol. 23, No. 3, pp.M -M , September, 1998.
4. Habchi, S., and Acharya, S., "Laminar Mixed Convection in a Partially Blocked, Vertical Channel," Int. J. Heat Mass Transfer, Vol. 29, pp. 1711-1722, 1986
5. Maughan J.R., and Incropera, F. P., "Experiments on Mixed Convection Heat Transfer for Air Flow in a Horizontal and Inclined Channel." I. J. Heat Mass Transfer. Vol. 30, pp. 1307-1318, 1987.
6. Kang. B. H., Jaluria, Y., and Tewari, S. S., "Mixed Convection Transport From an Isolated Heat Source Module on a Horizontal Plate," ASME J. of Heat Transfer, Vol. 112, pp. 653-661, 1990.
7. Mahaney, H., Incropera, F., and Ramadhyani, S., "Comparison of Predicted and Measured Mixed Convection Heat Transfer From an Array of Discrete Sources in a Horizontal Rectaugular Channel," Int. J. Heat Mass Transfer, Vol. 33, No. 6, pp. 1233-1245, 1990
8. Kim, S., Sung, H., and Hyun, J., "Mixed Convection From Multiple-Layered Boards With Cross-Streamwise Periodic Boundary Conditions," Int. J. Heat Mass Transfer, Vol. 35, No. 11, pp. 2941-2952, 1992
9. Patankar, S., "Numerieal Heat Transfer and Fluid Flow" Me Graw Hill, New York, 1980.